Attenuation of photons at 3–14-keV energies in helium

Y. Azuma,* H. G. Berry, D. S. Gemmell, and J. Suleiman†
Physics Division, Argonne National Laboratory, Argonne, Illinois 60439

M. Westerlind and I. A. Sellin
Department of Physics, University of Tennessee, Knoxville, Tennessee 37996
and Oak Ridge National Laboratory, Oak Ridge, Tennessee 37831

J. C. Woicik
National Institute of Standards and Technology, Gaithersburg, Maryland 20899

J. P. Kirkland
SFA Inc., 1401 McCormick Drive, Landover, Maryland 20785
(Received 14 July 1994)

We have measured the total photoattenuation cross section of helium for photons in the energy range of 3–14 keV. At these energies, the photoionization cross section is rapidly decreasing, so that Compton scattering is significant at 4 keV and dominates at the highest energies. Our measurements verify the dominance of Compton scattering in this energy range, and its importance in recent measurements of the ratio of double to single photoionization of helium. The measured cross sections are close to the combined calculated cross sections for Compton scattering and photoionization; we are able to distinguish the contributions of the two effects.

PACS number(s): 32.80.Cy, 32.80.Fb

I. INTRODUCTION

The photoionization cross section for helium decreases rapidly with energy above the 1–2-keV region. Most theories (see below) predict that it decreases asymptotically at high photon energies with the inverse seven-halves power of the photon energy. Consequently, other processes become important at photon energies above 2 keV, as pointed out in a recent Letter [1] and in a Comment [2]. Besides the photoionization process resulting in complete absorption of the incident photon, coherent and incoherent scattering of the incident photon can also occur. In particular, the Compton (incoherent) scattering cross section for helium is a few barns in this energy range and of the same order of magnitude (or larger) as that of the photoionization process. In addition, the coherent, Rayleigh scattering cross section (where the scattered radiation is the same wavelength as the incident radiation) is also a few barns in the 1–3-keV energy range. Thus the attenuation cross section is the sum

$$\sigma(\text{attenuation})=\sigma(\text{photoionization}) +\sigma(\text{Rayleigh})+\sigma(\text{Compton})\ . \quad (1)$$

At high enough incident photon energies, both single and double ionization can also occur in the Compton process, and hence also affect the relative yields of singly to doubly charged helium. At 12 keV, it is estimated that most of the attenuation results from Compton scattering.

Existing photoabsorption measurements in helium above approximately 200 eV are sparse and of low precision. In a recent review Samson *et al.* [3] assess the existing data for photoionzation. Experimental values show good agreement to within 1% up to about 200 eV, and Samson *et al.* [3] give suggested extrapolated values to the higher-energy range up to 10 keV. An important experimental difficulty has been the smallness of the cross section at these high photon energies, approximately seven orders of magnitude less than at threshold. Figure 1 shows the strongly decreasing attenuation cross section for helium, as given by the tabulations of Samson *et al.* [3], and of Marr and West [4], and all previously known measurements in the high-energy range [5–10]. Our objective in this paper is to test the validity of existing calculations for both Compton scattering and photoabsorption and compare them with experiment in the energy range of 3–14 keV. We have achieved a precision of 1–2 % in these measurements in order to be able to distinguish between the different calculations for both the photoionization and the Compton process. This precision has not been attained in measurements of photoattenuation for any other atom over any considerable energy range.

In Fig. 2, we show a curve representing a calculation by Veigele [11] of the Compton (incoherent) plus Rayleigh (coherent) scattering. We note that their sum exceeds the photoionization cross section at a photon energy of 6 keV, and at 14 keV, the highest-energy point of our measurements, it represents 98% of the total attenuation cross section. Hence, our work also provides a test of the Compton scattering calculations in the higher

*Present address: National Laboratory for High Energy Physics (KEK), 1-1, Oho, Tsukuba, Ibaraki, Japan 305.
†Also at the Department of Physics, University of Illinois, Chicago, IL 60607.

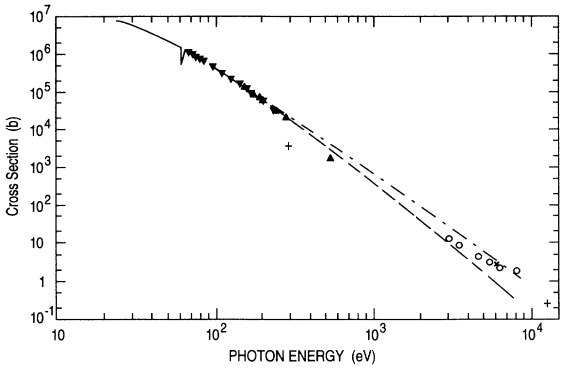

FIG. 1. The attenuation cross section of helium from threshold to 15 keV. The continuous line is a recommended fit from Samson *et al.* [3] and the dot-dashed curve is the compilation of Marr and West [4]. Measurements are from Denne [5] (▲); Watson [6] (▼); Bearden [7] (○); McCrary, Looney, and Atwater [8] (×), Messner [10] (+, at 300 eV); and Allen [9] (+, at 11 keV).

10–14-keV energy range.

Levin *et al.* [12,13] have recently measured the ratio of photoproduction of doubly to singly charged helium ions in the photon energy range of 2–12 keV. Other measurements for this ratio have also been completed recently, mostly at lower photon energies [14,15]. The measurements [12,13], showed some disagreements with existing calculations [16–20], and prompted several new calculations [21–25]. Since most methods of calculation agree that single- and double-photoionization cross sections are both proportional to the inverse seven-halves power of the photon energy at these high energies, the ratio should approach a constant. The value of this constant as measured in the higher-energy experiments [12,13] is close to 1.6%, and most new predictions cluster around this value. In the last few months three calculations of this ratio for Compton scattering have been published [1,26], and several calculations are in progress [27]. Our measurements reported here can then clarify the importance of Compton scattering in this energy range, and affirm the role of Compton scattering in the charge-state ratio measurements of Levin *et al.* [12,13].

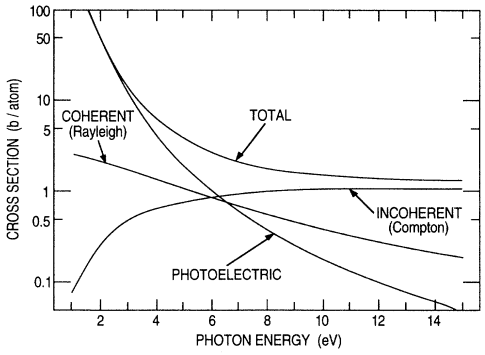

FIG. 2. Calculations by Veigele [11] of the photoionization (photoelectric), Rayleigh (coherent), and Compton (incoherent) cross sections as functions of photon energy.

II. EXPERIMENT

X-ray attenuation measurements in gases have been made for almost 100 years. The major difficulty for helium measurements in this photon energy range of 3–14 keV is the extremely small attenuation coefficient, with a total cross section going down to less than two barns. In this same energy range other gases typically have absorption cross sections of up to a megabarn, and hence the experiments can easily be affected by impurities. For our experiment we used 99.9999% pure, neon-free helium. The gases in this remaining 1 ppm would yield effective attenuations of less than 1% of our measured values, based on known compiled cross-section values [28]. The measurements thus give an upper limit to the attenuation cross section, since any impurity except for hydrogen would tend to increase the measured cross sections.

Our measurements took place at three beamlines of the x-ray ring of the National Synchrotron Light Source at Brookhaven National Laboratory. The early measurements at 4.5–8-keV beam energies were made at the Naval Research Laboratories' X-23B beamline. The X-24A beamline, jointly operated by the National Institute of Standards and Technology (NIST), and the Physics Division at Argonne National Laboratory, provides a well-focused and monochromatized beam of photons and was used in the energy range of 2–5.5 keV. The X-23A2 beamline, operated by NIST, provides a monochromatized beam in the energy range of 5–14 keV. Figure 3 shows the experimental layout for the X-24A beamline.

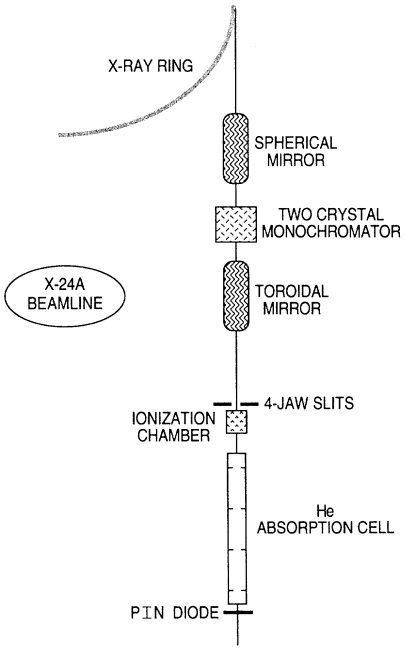

FIG. 3. A schematic illustration of the experimental arrangement for measurements at the X24A beamline. The experimental arrangements were similar at the other beamlines.

The apparatus consists of a 1.4 m long helium absorption tube, 5 cm in diameter, with 75×10^{-6} m thick, 7 mm diameter, Kapton (Kapton is a trade mark of Du-Pont De Nemours EI&Co.) windows on each end. The tube is connected to a gas-handling system, and could be filled with helium up to a pressure of 10^6 Pa. The whole system was pumped out initially to better than 3×10^{-5} Pa. Pressure and vacuum gauges with electronic readouts allowed us to monitor the pressure absolutely to better than 1% at all pressures, and to record the pressure simultaneously to each photoabsorption measurement. The length of the absorption path was measured to be $L=139.38\pm0.05$ cm. The number of helium atoms in the light path at a pressure p and temperature T is

$$N(\mathrm{He})=\frac{p(\mathrm{Pascal})}{T(\mathrm{K})}\frac{273}{760}\frac{6.022\times10^{23}}{22.4\times10^{3}}\frac{1}{133.2}\ \mathrm{atoms\,cm^{-3}}\ . \quad (2)$$

For an attenuation cross section σ, the logarithmic ratio of initial intensity I_0 and final intensity I becomes

$$\ln\left[\frac{I_0}{I}\right]=\sigma LN=7.250\times10^{16}\sigma(\mathrm{cm^{-2}})\frac{L(\mathrm{cm})}{T(\mathrm{K})}p(\mathrm{Pa})\ . \quad (3)$$

A neon-filled ionization chamber was used to record the photon flux upstream of the helium absorption tube, and a *p-i-n* diode monitored the flux following the absorption tube. The ratio of these two signals provides the raw absorption data. The *p-i-n* diode was operated as suggested in the work of Kirkland *et al.* [29], its signal being amplified and converted to a pulse rate by a model RN811 bipolar charged pump digitizer (red nun). Four-jaw slits just in front of the ionization chamber defined the photon beam size, typically 1 mm square, within the chamber. The position of the *p-i-n* diode could be adjusted vertically and horizontally so that it was in the center of a signal plateau region. The temperature was recorded for each measurement. Temperature changes (mostly diurnal variations) were significant, with variations of up to 5 °C being observed and accounted for during the measuring periods.

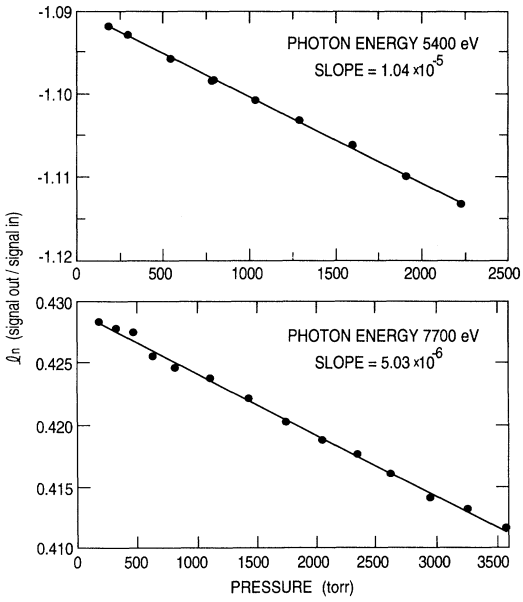

FIG. 4. The transmission of light through the helium absorption tube as a function of pressure for two photon energies, 5400 and 7700 eV.

The crystal monochromator, its distance to the four-jaw slits, and their aperture width of 1 mm, combined to give an energy resolution of $\Delta E/E\approx2\times10^{-4}$ over the respective energy ranges of the different beamlines.

The absorption tube was fitted with six equally spaced axial disks each with a 7 mm diameter aperture centered on the tube axis. These baffles were included to minimize scattered x rays from reaching the *p-i-n* diode detector. Secondary ions, electrons, and Compton photons could produce such radiation on impact with the chamber walls. No direct view of these surfaces from the *p-i-n* diode was possible.

At each photon energy we measured the absorption ratio for typically 10–15 helium pressures ranging between 10^4 and 8×10^5 Pa. Figure 4 shows some typical semilogarithmic absorption curves. Each linear fit gives an estimated uncertainty for the measured slope. Each slope is proportional to the attenuation cross section at the given photon energy [Eq. (3)]. Several measurements were made at similar pressures to allow an estimate of uncertainties in the measured cross sections.

The photon energies from each beamline monochromator were calibrated using known K-edge absorption energies. The argon K edge was used to calibrate the low-energy measurements, 3–5.5 keV, at the X24A beamline. Metallic absorption edges (Cu at 8979 eV, Cr at 5989 eV, and Nb at 6329 and 18 986 eV) were used to calibrate the higher energies at the X-23A2 beamline. The niobium K edge was used to check the intensity of the third-order harmonic at 3×6329 eV, and showed that its intensity was less than 1%.

III. RESULTS

Each attenuation curve, similar to those shown in Fig. 4, was fitted with a linear regression to the logarithmic decay. The slope is proportional to the attenuation cross section, as given in Eq. (2) above. Such analysis generally gave a fitted slope parameter with an estimated precision between 0.01% and 0.1%. Any nonlinearity due to beam position or intensity variations or other origin leads to a lower fitting precision and such data were removed from further analysis. In Table I we list the results obtained for the attenuation cross section for helium between 3200 and 14 000 eV. Most of the data values correspond to an average of several measurements at each listed energy. The error bars lie between 1% and 2% of the measured value and depend slightly on the conditions at each energy. Thus, at the higher energies, the reduced photon flux and the low cross sections contribute significantly to a slight loss in precision. The quoted errors reflect the reproducibility of the measurements at each energy.

TABLE I. Measured and calculated helium absorption cross sections in the energy range of 3–14 keV. The cross sections are given in barns (10^{-24} cm^{-2}). The number(s) in parentheses in column 2 represent the uncertainty in the last 1 (2) digit(s). The fitted total cross section given in the last column includes photoionization, incoherent, and coherent processes.

Energy (eV)	Measured cross section $\sigma_{expt}(E)$	Fitted (cubic) coh.+incoherent cross section σ_{IC}	σ_{ph} (expt) $=\sigma_{expt}(E)-\sigma_{IC}$	σ_{ph}(hydrogen) $Z_{eff}=1.83$	Fitted total cross section
3 350	9.75(10)	2.14	7.61	7.57	9.71
3 550	8.07(8)	2.11	5.96	6.08	8.19
3 750	6.93(7)	2.07	4.87	4.94	7.01
3 950	6.05(7)	2.04	4.01	4.06	6.10
4 150	5.26(5)	2.01	3.25	3.37	5.38
4 350	4.66(5)	1.97	2.69	2.82	4.79
4 550	4.16(5)	1.94	2.22	2.38	4.32
4 750	3.79(5)	1.92	1.85	2.02	3.94
4 950	3.55(5)	1.89	1.66	1.73	3.62
5 150	3.30(5)	1.86	1.44	1.49	3.45
5 350	3.11(5)	1.84	1.27	1.29	3.13
5 500	3.07(4)	1.82	1.25	1.16	2.98
5 550	2.93(4)	1.81	1.12	1.12	2.93
6 000	2.57(4)	1.76	0.81	0.84	2.60
6 500	2.41(4)	1.71	0.70	0.62	2.33
7 000	2.14(4)	1.67	0.43	0.47	2.14
8 000	1.84(3)	1.60	0.24	0.28	1.88
9 000	1.70(3)	1.55	0.15	0.18	1.73
10 000	1.61(3)	1.51	0.10	0.12	1.63
11 000	1.56(4)	1.49	0.06	0.08	1.57
12 000	1.48(3)	1.47	0.01	0.06	1.53
13 000	1.47(2)	1.46	0.01	0.05	1.51
14 000	1.41(4)	1.40	0.01	0.04	1.44

The measured cross sections are also plotted semilogarithmically as a function of photon energy in Fig. 5. We also show other experimental data in this region, from Bearden [7], from McCrary, Looney, and Atwater [8], and from Allen [9], and compare these data with the calculations of Veigele [11]. In Table II we compare the same measured attenuation cross sections with three calculations of Veigele [11], Hino [21], and Andersson and Burgdörfer [1].

IV. ANALYSIS OF THE ATTENUATION RESULTS

In Fig. 5, we also indicate other available experimental data. Bearden [7] (solid triangles, vertex up) indicated in his paper an uncertain impurity content in his helium gas of about 0.03% nitrogen. Because of the much higher cross section for nitrogen in this energy region, it can increase the measured cross section. Assuming Bearden's stated impurity content, we have "corrected" the cross section as suggested by Samson [3], using published nitrogen cross sections [30]. The results are indicated by triangles (vertex down). McCrary, Looney, and Atwater [8] made a single attenuation measurement at 5.9 keV photon energy. Their value of 2.77±0.11 barns is extracted and quoted in the compilation of Saloman, Hubbell, and Scofield [30].

Although several earlier calculations and compilations exist for the helium-ionization coherent and incoherent cross sections [31], the results are very similar to the more complete tabulations of Veigele [11], and we have used principally Veigele's calculations for an interpretation of the data. Veigele [11] uses the Hartree-Fock self-consistent-field method to calculate the photoionization cross sections in the range below 10 keV, and adds the Compton cross sections of Cromer and Mann [32] for the Compton scattering part. McCrary, Looney, and Atwater [8] obtain identical results. Two recent calculations for the relevant cross sections have been published by Andersson and Burgdörfer [1], and by Hino and co-

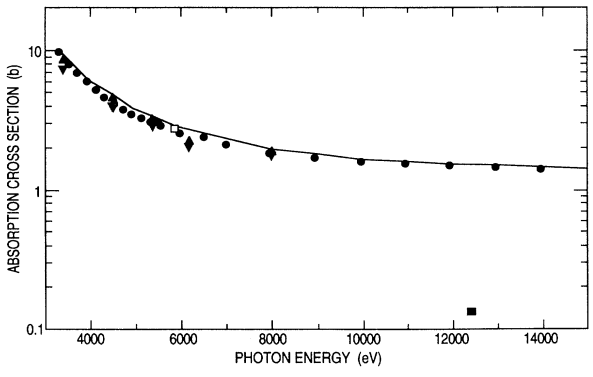

FIG. 5. The total attenuation cross section for helium as a function of photon energy. Our measurements are bullets (●). The original and revised measurements of Bearden [7] are the triangles (▲) and (▼), respectively. Other measurements are from McCrary, Looney, and Atwater [8] (□), and Allen [9] (■). The solid line is the theoretical calculation of Veigele [11].

TABLE II. Comparison of the measured attenuation cross sections with three calculations, taken from Refs. [11], [21], and [1] and also with a recent compilation of Cullen *et al.* [35]. The experimental values are the same as listed in Table I, where error limits are included. The theoretical values are those used in obtaining the cubic fits listed in Table I. The calculations include photoionization, coherent, and incoherent processes.

Energy	Total cross sections (b)				
(eV)	Veigele [11]	Hino [21]	Andersson [1]	Cullen [35]	This experiment
2 000	44.90	43.05	42.17	45.37	
2 500				22.76	
3 000	13.29		12.70		
3 350					9.75
3 500				8.73	
3 550					8.07
3 750					6.93
3 950					6.05
4 000	6.23	6.10	6.03	6.23	
4 150					5.26
4 350					4.66
4 550					4.16
4 750					3.79
4 950					3.55
5 000	3.84		3.75	3.83	
5 150					3.30
5 350					3.11
5 500				3.22	3.07
5 550					2.93
6 000	2.80	2.77	2.76		2.57
6 500					2.41
7 000				2.25	2.14
8 000	1.98	1.97	2.00	1.95	1.84
9 000				1.77	1.70
10 000	1.66	1.66		1.64	1.61
11 000				1.56	1.56
12 000					1.48
13 000					1.47
14 000				1.42	1.41
15 000	1.40				
16 000				1.36	

workers [21,33], and we have also made careful comparisons with their results.

Figure 6 compares the results of these three calculations over the high-energy range. The three calculations agree to well within 1%, and the three sets of points are barely separable on the plot. At nonrelativistic energies the Klein-Nishina formula for Compton scattering reduces to the classical incoherent Thomson scattering cross section. The Thomson scattering cross section for photons from a free electron is $\frac{8}{3}\pi r_0^2 = 0.666$, or 1.33 b for the two electrons per atom.

In addition, we note that Fig. 5 and Tables I and II show that although the experimental total attenuation cross sections tend to lie below the calculations of Veigele, there is better agreement at high energy, above 10 keV, where the Compton cross section dominates. We conclude that experiment and theory all agree on values for the Compton cross section above 10 keV to better than ±2%. Therefore we make a substraction from the experimental data of the Compton and Rayleigh scattering to obtain a residual photoionization (photoelectric-

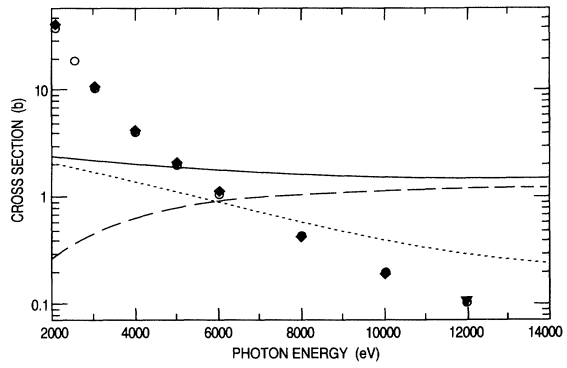

FIG. 6. The coherent (Rayleigh) and incoherent (Compton) scattering cross sections of Veigele [11], of Hino and McGuire [21], and of Andersson and Burgdörfer [1] agree closely, and are represented by the short-dashed and the long-dashed lines, respectively, of the cubic fits. Their sum is the solid line. The three calculations of the photoionization cross sections of the same authors are given: Ref. [1] (open circles), Ref. [11] (solid diamonds), and Ref. [21] (solid triangles).

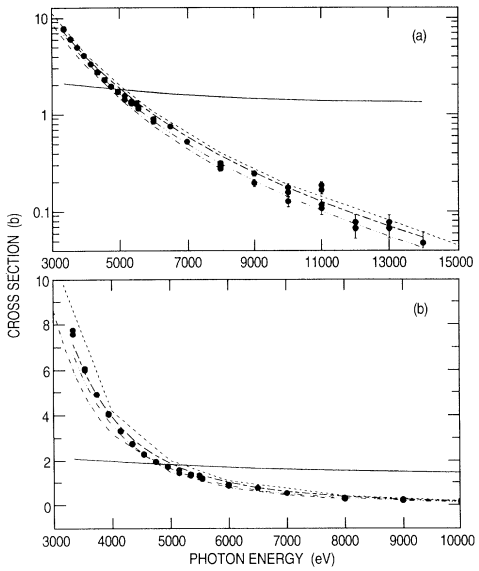

FIG. 7. The photoelectric cross section for helium: (a) logarithmic and (b) linear plot. The symbols are from experiment (the averaged values are given in Table I). The lines are as follows: solid, Compton cross section; dot-dashed, Ref. [3]; short dashes, Ref. [11]; short dash–long dash, Eq. (3) with $Z=1.837$ (fit); three dots–one dash, 460×(photon energy to the power of −3.5).

absorption) cross section $\sigma_{\rm ph}$. The results are given in column 4 of Table I. Since theoretical results are not available for all the measured energies, the subtraction was made by first fitting the theoretical Veigele cross section (the sum of the coherent and incoherent parts) to a cubic function $a+bE+cE^2+dE^3$, where E is the energy in eV, and subtracting this function from the data. The constants for the coherent and incoherent parts are given in Table III.

Figures 7(a) and 7(b) compare the measured photoelectric cross sections with several calculations. The logarithmic and linear scales are used to clarify the differences at low and high energies. First we note the calculations of Veigele are systematically higher than the data by 2–5%. The calculations of Andersson and Burgdörfer [1] (not shown) are closer to the curve of Veigele [11] than the data. Impurities in the helium gas would yield too high a measured cross section, further away from theory than the present results.

The other curves of Fig. 7 represent fits to the data. The fit of Samson *et al.* [3] derived from existing lower-energy data appears to be too low in this region. A fit of the data to the inverse seven-halves power of the photon energy, $\sigma(\text{b})=kE(\text{keV})^{-7/2}$, the standard limiting power law predicted by most calculations, yields a coefficient of $k=460$. This is significantly different from that of Samson, Greene, and Bartlett [2], $k=410$.

We have made a fit to the data by generalizing the hydrogenic formula for photoionization:

$$\sigma=\frac{2^6\pi}{3\sqrt{2}}\frac{Z^5}{c}\frac{1}{E^{7/2}}(1-\pi\sqrt{I_{1s}/E}\,)\,, \tag{4}$$

TABLE III. Parameters in the cubic function $a+bE+cE^2+dE^3$ fitted to represent the coherent and incoherent cross sections. E is the photon energy in eV, and the cross sections are in barns (10^{-24} cm^2).

Parameter (units)	Coherent cross section	Incoherent cross section
a (b)	3.18	−0.2048
b (b eV^{-1})	-5.82×10^{-4}	2.63×10^{-4}
c (b eV^{-2})	4.05×10^{-8}	-1.76×10^{-8}
d (b eV^{-3})	-9.7×10^{-13}	4.06×10^{-13}

where c is the velocity of light, Z is the nuclear charge, and I_{1s} is the ionization potential. Replacing the nuclear charge by a screened value $Z\rightarrow Z_{\rm eff}$, we fit the data to the parameter $Z_{\rm eff}$, which yields a value $Z_{\rm eff}=1.837$. This curve gives an excellent fit to our results as shown in Fig. 5. We note that the second term in Eq. (4) is important in an accurate presentation of the photoelectron cross section in this region, since it still gives a few percent contribution at 10 keV. For example, the Veigele values for this cross section are also much better fitted by the two-term formula than the single $E^{-7/2}$ term, but with a slightly higher value for $Z_{\rm eff}$.

We conclude these attenuation measurements with a recommended attenuation cross section for helium which should be accurate up to at least 15 keV photon energy. Below 2 keV, the compilation of Samson is satisfactory. Above this energy, the photoionization cross section is well represented by Eq. (4), with an effective nuclear charge of $Z=1.837$. To this value one needs to add the sum of the incoherent and coherent cross sections which are well represented by the cubic functions with parameters given in Table III. The results agree well with our data of Table I throughout this energy range.

V. CONCLUSIONS

We note that we have been able to show that the Compton cross section is important at energies above 2 keV to explain the measured attenuation cross sections for helium, and to verify the existing calculations. An initial measurement of momentum transfer in Compton scattering by helium has just been published [34]. More accurate measurements of the doubly to singly charged helium ion production ratio around 4–8 keV might reveal this threshold for He^{2+} production in Compton scattering; and more calculations of the expected charge ratio in Compton scattering in this energy region would be helpful for further interpretation.

ACKNOWLEDGMENTS

We thank Miron Amusia for many helpful discussions especially on the role of Compton scattering in the attenuation process. We acknowledge the help of Barry

Karlin in the measurements at the NSLS X24A beamline. This research was supported by the U.S. Department of Energy, Fundamental Interactions Branch, Office of Basic Energy Sciences, Division of Chemical Sciences, under Contract No. W-31-109-ENG-38 (Argonne), and the National Science Foundation (Tennessee), and under Contract No. N0014-92-C-2254 for the Naval Research Laboratory (J.P.K.).

[1] L. R. Andersson and J. Burgdörfer, Phys. Rev. Lett. **71**, 50 (1993).
[2] J. A. R. Samson, C. H. Greene, and R. J. Bartlett, Phys. Rev. Lett. **71**, 201 (1993).
[3] J. A. R. Samson, Z. X. He, L. Yin, and C. N. Haddad, J. Phys. B **27**, 887 (1994).
[4] G. V. Marr and J. B. West, At. Data Nucl. Data Tables **18**, 497 (1976).
[5] D. R. Denne, J. Phys. D **3**, 1392 (1970).
[6] W. S. Watson, J. Phys. B **5**, 2292 (1972).
[7] A. J. Bearden, J. Appl. Phys. **37**, 1681 (1966).
[8] J. H. McCrary, L. D. Looney, and H. F. Atwater, J. Appl. Phys. **41**, 3570 (1970). McCrary *et al.* also quote a measurement of M. Wiedenbeck, Phys. Rev. **126**, 1009 (1962), at 42.98 keV. However, the reference does not contain any attenuation measurements for helium. E. O. Wollan, Phys. Rev. **37**, 862 (1931), has made some angle-differential measurements of scattered photons in this region, but no attenuation measurements.
[9] S. J. M. Allen, in *X-rays in Theory and Experiment,* edited by A. H. Compton and S. K. Allison (Van Nostrand, New York, 1935), Appendix IX, Table I.
[10] R. H. Messner, Z. Phys. **85**, 727 (1933).
[11] W. J. Veigele, At. Data Tables **5**, 51 (1973).
[12] J. C. Levin, D. W. Lindle, N. Keller, R. D. Miller, Y. Azuma, N. Berrah-Mansour, H. G. Berry, and I. A. Sellin, Phys. Rev. Lett. **67**, 968 (1991).
[13] J. C. Levin, I. A. Sellin, B. M. Johnson, D. W. Lindle, R. D. Miller, N. Berrah, Y. Azuma, H. G. Berry, and D.-H. Lee, Phys. Rev. A **47**, R16 (1993).
[14] N. Berrah, F. Heiser, R. Wehlitz, J. Levin, S. B. Whitfield, J. Viefhaus, I. A. Sellin, and U. Becker, Phys. Rev. A **48**, R1733 (1993).
[15] J. C. Levin (private communication); M. Sagurton *et al.* (unpublished).
[16] F. W. Byron and C. J. Joachain, Phys. Rev. **164**, 1 (1967).
[17] T. Åberg, Phys. Rev. A **2**, 1726 (1970).
[18] M. Ya. Amusia, E. G. Drukarev, V. G. Gorshkov, and M. Kazachkov, J. Phys. B **8**, 1248 (1975).
[19] A. Dalgarno and A. L. Stewart, Proc. Phys. Soc. London **76**, 49 (1960); A. Dalgarno and R. W. Ewart, *ibid.* **80**, 616 (1962).
[20] S. L. Carter and H. P. Kelly, Phys. Rev. A **24**, 170 (1981); see Refs. [6] and [7] of this paper for a more complete listing of the early (pre-1990) calculations of the high-energy limit.
[21] T. Ishihara, K. Hino, and J. H. McGuire, Phys. Rev. A **44**, R6980 (1991); K. Hino, *ibid.* **47**, 4845 (1993).
[22] A. Dalgarno and H. R. Sadeghpour, Phys. Rev. A **46**, R3591 (1992).
[23] Z. J. Teng and R. Shakeshaft, Phys. Rev. A **47**, R3487 (1993); **49**, 3597 (1994).
[24] J. A. R. Samson, Phys. Rev. Lett. **65**, 2861 (1990).
[25] C. Pan and H. P. Kelly (unpublished).
[26] K. Hino, P. M. Bergstrom, and J. H. Macek, Phys. Rev. Lett. **72**, 1620 (1994); J. Burgdörfer, L. R. Andersson, J. McGuire, and T. Ishihara, Phys. Rev. A **50**, 349 (1994).
[27] M. Ya. Amusia (private communication); R. H. Pratt (private communication).
[28] J. A. Bearden, Rev. Mod. Phys. **39**, 78 (1967); J. A. Bearden and A. F. Burr, *ibid.* **39**, 125 (1967).
[29] J. Kirkland, T. Jach, R. A. Neiser, and C. E. Bouldin, Nucl. Instrum. Methods Phys. Res. Sect. A **266**, 602 (1988); T. Jach and P. L. Cowan, Nucl. Instrum. Methods Phys. Res. **208**, 423 (1983).
[30] E. B. Saloman, J. H. Hubbell, and J. H. Scofield, At. Data Nucl. Data Tables **38**, 2 (1988).
[31] J. H. Hubbell, W. J. Veigele, E. A. Briggs, R. T. Brown, D. T. Cromer, and R. Howerton, J. Phys. Chem. Ref. Data **4**, 47 (1975).
[32] D. T. Cromer and J. B. Mann, J. Chem. Phys. **47**, 1892 (1976).
[33] K. Hino, T. Ishihara, F. Shimizu, N. Toshmia, and J. H. McGuire, Phys. Rev. Rev. A **48**, 1271 (1993).
[34] J. A. R. Samson, Z. X. He, R. J. Barlett, and M. Sagurton, Phys. Rev. Lett. **72**, 3329 (1994).
[35] D. E. Cullen, M. H. Chen, J. H. Hubbell, S. T. Perkins, E. F. Plechary, J. A. Rathkopf, and J. H. Scofield, UCRL Report No. UCRL-50400, Vol. 6, part A, Rev. 4, 1989 (unpublished).

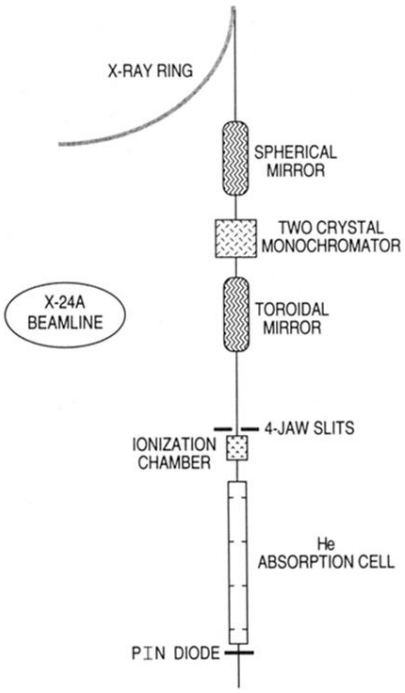

FIG. 3. A schematic illustration of the experimental arrangement for measurements at the X24A beamline. The experimental arrangements were similar at the other beamlines.